Published in final edited form as:
J Immunol. 2010 February 1; 184(3): 1328–1338. doi:10.4049/jimmunol.0903071.

Formation of a Mast Cell Synapse: FcεRI Membrane Dynamics upon Binding Mobile or Immobilized Ligands on Surfaces[1]

Amanda Carroll-Portillo[*,¶], **Kathrin Spendier**[‡], **Janet Pfeiffer**[*], **Gary Griffiths**[§], **Haitao Li**[§,3], **Keith A. Lidke**[‡], **Janet M. Oliver**[*], **Diane S. Lidke**[*], **James L. Thomas**[‡], **Bridget S. Wilson**[*,2], and **Jerilyn A. Timlin**[2,¶]

[*] Department of Pathology, University of New Mexico, Albuquerque, New Mexico 87131, USA

[‡] Department of Physics and Astronomy and Spatiotemporal Modeling Center, University of New Mexico, Albuquerque, New Mexico 87131, USA

[§] Imaging Probe Development Center, NIH, NHLBI, Bethesda, MD 20892

[¶] Biofuels and Defense Technologies, Sandia National Laboratories, Albuquerque, New Mexico 87185-0895

Abstract

High affinity IgE receptors (FcεRI) on mast cells form a “synapse” when presented with mobile, bilayer incorporated antigen. Here, we show that receptor reorganization within the contacting mast cell membrane is markedly different upon binding of mobile and immobilized ligands. Rat basophilic leukemia mast cells (RBL-2H3) primed with fluorescent anti-DNP IgE were engaged by surfaces presenting either bilayer-incorporated, monovalent DNP-lipid (mobile ligand) or chemically crosslinked, multivalent DNP (immobilized ligand). Total internal reflection fluorescence imaging and electron microscopy methods were used to visualize receptor reorganization at the contact site. The spatial relationships of FcεRI to other cellular components at the synapse, such as actin, cholesterol and LAT, were also analyzed. Stimulation of mast cells with immobilized polyvalent ligand resulted in typical levels of degranulation. Remarkably, degranulation also followed interaction of mast cells with bilayers presenting mobile, monovalent ligand. Receptors engaged with mobile ligand coalesce into large, cholesterol-rich clusters that occupy the central portion of the contacting membrane. These data indicate that FcεRI crosslinking is not an obligatory step in triggering mast cell signaling and suggest that dense populations of mobile receptors are capable of initiating low level degranulation upon ligand recognition.

Keywords

Immunological Synapse; IgE; FcεRI; LAT; cholesterol

[1]This work was supported in part by the Laboratory Directed Research and Development program at Sandia National Laboratories (JAT), by NIH R01AI051575 (BSW), by the Human Frontiers Science Program (DSL), by the Army Research Office Grant W911NF0510464 (KS), and by NIH P50GM085273 supporting the New Mexico Spatiotemporal Modeling Center. Sandia is a multiprogram laboratory operated by Sandia Corporation, a Lockheed Martin Company, for the US Dept. of Energy’s National Nuclear Security Administration under Contract DE-AC04-94AL85000. The Cancer Center Fluorescence Microscopy Facility received support from NCRR 1 S10 RR14668, NSF MCB9982161, NCRR P20 RR11830, NCI P30 CA118100, NCRR S10 RR016918, the UNM Health Sciences Center and the UNM Cancer Center.

[2]Address correspondence and requests for reprints to Dr. Bridget S. Wilson, Department of Pathology and Cancer Center, University of New Mexico Health Sciences Center, Albuquerque, NM 87114. bwilson@salud.unm.edu or Dr. Jerilyn Timlin, Sandia National Laboratories, Albuquerque, NM 87185. jatimli@sandia.gov.
[3]Current address: Office of Generic Drugs, Division of Chemistry III, Rockville, MD 20855

Introduction

In basophils and mast cells, crosslinking of IgE bound to its cognate high affinity receptor, FcεRI, triggers release of histamine and other mediators of allergic inflammation. Activated receptors are phosphorylated by Lyn, a membrane-tethered Src-family kinase, on tyrosine residues within ITAM domains of the FcεRI β and γ subunits. Syk is subsequently recruited to receptor complexes (1) through interactions of its tandem Src homology 2 (SH2) domains with ITAMs in the FcεRI γ subunits (2, 3). Syk activation enables propagation of a signaling cascade to downstream components such as LAT, PLCγ and NFAT (4). Signaling is absent in cells lacking Syk (5–7) and delayed in cells lacking Lyn (8), suggesting that other kinases can replace Lyn, albeit inefficiently, and that Syk activation is essential for signaling.

The multi-subunit immunorecognition receptor (MIRR) family to which FcεRI belongs also includes the TCR and the BCR. Upon activation by antigen binding, these immunoreceptors also employ Src and Syk family kinases to initiate a phosphorylation cascade for signaling (9–11). Contact between lymphocytes bearing these receptors and either lipid bilayers or antigen presenting cells bearing ligand leads to formation of an immunological synapse (12–17). Well known aspects of lymphocyte immune synapses include aggregation of receptor-ligand complexes at the center of the contact site and redistribution of integrins to the periphery. These spatial interactions serve to bridge the two cells and control the responsiveness of signaling.

Here, we explore the potential for mast cells to form synapses when presented with antigen on surfaces, analogous to the responses of T cells and B cells. Work in the 1980s by the McConnell and McCloskey laboratories established that liposomes bearing haptens for IgE could mediate adhesion to RBL-2H3 mast cells and provide lateral forces that induced both FcεRI clustering and serotonin release (18, 19). More recently, Silverman and colleagues described punctate clustering of FcεRI after settling of mast cells on coverslips coated with polyvalent antigen, accompanied by recruitment of Syk and SLP-76 (20). Evidence for direct contacts between mast cells and other immune cells (21–23) indicates that mast cell synapses may play a role in inflammatory responses. Here, transmission electron microscopy (TEM) and total internal reflection fluorescence (TIRF) imaging were combined to more closely examine the spatial relationships of components at the mast cell synapse, including FcεRI, the adaptor LAT, cholesterol and actin. We show that relationships between these components at the membrane interface differ significantly, depending upon the mobility of ligands on the contact surface. IgE-primed receptors bound to mobile, monovalent ligand form large, centralized, mobile, cholesterol-rich clusters that can initiate weak, but measurable signaling (as detected by β-hexosaminidase release) despite the lack of direct crosslinking. Strong signaling to secretion results when IgE-FcεRI complexes are bound to surfaces presenting immobilized, polyvalent ligand. Cholesterol co-localization is markedly lower in the latter case, suggesting that cholesterol trapping does not accompany the immobilization of receptors.

Materials and Methods

Reagents and cell culture

RBL-2H3 and GFP-actin RBL-2H3 cells were maintained in MEM (Invitrogen; Carlsbad, CA) supplemented with 10% fetal bovine serum, penicillin-streptomycin, and L-glutamine. Affinity purified anti-DNP IgE (IgE^{DNP}) was prepared as previously described (24, 25). Fluorescent IgE conjugates were created using N-hydroxysuccinimide esters of Alexa 488 (Invitrogen; Carlsbad, CA) or Dy-520XL (Dyomics GmbH; Germany). Mouse anti-FcεRI β and anti-FITC monoclonal antibodies were gifts of Dr. Juan Rivera (NIH, Bethesda, MD) and Dr. Larry Sklar (Univ. of New Mexico) respectively. Anti-LAT antibodies (Santa Cruz

Biotechnology; Santa Cruz, CA) were used in electron microscopy studies and anti-phosphoLAT antibody (pY191; Epitomics; Burlingame, CA) was used in immunofluorescence.

Exocytosis Assay

β-hexosaminidase release was measured as previously described (26). Briefly, 2×10^5 suspension cells were primed for 2–24 hrs with 1 μg/ml IgE^{DNP}, then washed and re-suspended in HBBS. Primed cells were permitted to settle onto triplicate wells of 24-well plates pre-coated with mobile or immobile ligands, and incubated for 30 min at 37°C. Supernatants were then collected for degranulation assays. Data are presented as percent of total β-hexosaminidase content released into the medium over 30 min.

Generation and characterization of immobilized/mobile hapten surfaces

Immobilized DNP surfaces—Dinitrophenol-conjugated bovine serum albumin (DNP_{24}-BSA at 1 μg/ml; Invitrogen; Carlsbad, CA) or Nε-(2,4-Dinitrophenyl)-L-lysine hydrochloride (DNP-lysine at 10 μg/ml; Sigma; St. Louis, MO) were immobilized through crosslinking to poly-L-lysine-coated coverslips or TEM grids with a homobifunctional crosslinker [Ethylene glycol bis(succinimidylsuccinate), EGS (Fisher; Rockford, IL)]. Reactions were quenched with 100 mM glycine in PBS and prepared coverslips were stored in buffer until use.

Mobile surfaces—Liposomes composed of 1.3 mM 1-Palmitoyl-2-Oleoyl-*sn*-Glycero-3-Phosphocholine (POPC) and 0–25 mol% of N-Dinitrophenyl-aminocaproyl Phosphatidylethanolamine (DNP-Cap PE) (Avanti Lipids; Alabaster, AL) were made by hydrating lipid films in PBS, 2 mM Mg^{2+} followed with sonication. Supported lipid bilayers containing DNP-lipid were generated from liposomes on coverslips or electron microscopy grids via liposome fusion at 37°C and maintained at temperature for experiment duration.

Fluorescence Recovery after Photobleaching (FRAP)

The mobility of IgE bound to DNP-lipid containing bilayers was measured by FRAP using a Zeiss LSM510META confocal microscope with a 63×1.4 NA oil immersion objective. Bilayers were composed of POPC:DNP-Cap PE with 3 mol% *N*-(4,4-difluoro-5,7-dimethyl-4-bora-3a,4a-diaza-*s*-indacene-3-propionyl)-1,2-dihexadecanoyl-*sn*-glycero-3-phospho-ethanolamine, triethylammonium salt (BODIPY®FL DHPE; Invitrogen; Carlsbad, CA). Images were acquired at 400–800 ms/frame using low power 488nm excitation. A circular region with a 2.5 μm diameter was photobleached by increasing the laser to 95% power for 5 sequential scans, followed by recovery. Post-bleach curves were fit in MATLAB (The MathWorks, Natick, MD) to estimate the half-time and diffusion coefficients according to a linearizing method developed by Yguerabide et al. (27). FRAP images of the mast cell synapse were acquired on a custom hyperspectral confocal microscope (28) using 488 nm excitation through a 60× oil-immersion objective (Nikon, PlanApo VC NA = 1.40) at a rate of 4167 spectra/sec. Laser power at the sample was ~100 μwatts. A 12 μm × 12 μm region encompassing a corner of the synapse and a portion of surrounding area was photobleached by 15 repetitive scans. Recovery scans were taken at 6 and 8 minutes post-bleach. Resulting images were corrected for dark current and offset contributions and the spectral information from 515 nm to 585 nm was binned to produce the final images for recovery analysis.

Total Internal Reflection Fluorescence (TIRF) imaging

Coverslips with mobile or immobilized ligands were transferred to temperature-controlled chambers (Warner instruments; Hamden, CT). Cells were prelabeled with $IgE^{Alexa488}$ or

IgE^{Dy520}, allowed to settle onto coated surfaces and maintained at 37°C throughout the experiment. Objective-based TIRF imaging was performed as previously described (29) using excitation from a 488-nm continuous wave laser (Model 5450-00C, Ion Laser Technology, Inc.; Salt Lake City, UT) into an inverted microscope (Olympus IX 71, Olympus America Inc.; Center Valley, PA) equipped with an electron multiplied CCD detector (iXon 887, Andor Technologies, Inc.; Belfast, Northern Ireland) and a 60× TIRF oil objective (Olympus America Inc.; Center Valley, PA) plus 1.6× magnification in the microscope beam path for a final magnification of 90×. An image splitter (OptoSplit II, Cairn Research Ltd.; United Kingdom) allowed for simultaneous imaging of two spectrally distinct fluorescent labels (AF488, FITC, or GFP in combination with Dy520 XL). Image processing was performed with in house software implemented in MATLAB (The MathWorks, Inc.; Natick, MA) in conjunction with the image processing library DIPImage (Delft University of Technology; Delft, The Netherlands).

Epifluoresence and Brightfield Imaging

To estimate surface binding efficiency, EGS-DNP_{24}-BSA and 25 mol% DNP-lipid bilayers were prepared in 8-well Lab-Tek chambers (Nunc/Thermo Fisher; Rochester, NY). IgE^{DNP}-primed RBL cells (1×10^5) were allowed to settle onto each surface for 12 minutes at 37°C. Ten different fields of view were captured using brightfield microscopy with a 63×1.4 NA oil immersion objective. Average percentage of cells bound to the surface was determined for each surface tested. To evaluate actin and protein reorganization at the synapse, IgE^{AF488} primed RBL cells in HBSS were settled onto EGSDNP_{24}-BSA, 25 mol% DNP-lipid bilayers or bare glass for 6 or 12 minutes at 37°C. Samples were fixed using 4% paraformaldehyde and 0.1% Triton X-100 and stained for either rhodamine phalloidin (Invitrogen; Carlsbad, CA) or phospho-LAT and FcεRI β. Samples were imaged on a LSM 510META confocal microscope with a 63× 1.4 NA oil immersion objective.

Single particle tracking

$IgE^{Alexa488}$ on primed cells or bound alone to DNP-lipid containing bilayers imaged in TIRF was tracked with the ImageJ (National Institutes of Health, Bethesda, MD) SpotTracker plug-in (30) for 15 and 25 seconds respectively. The two dimensional mean squared displacement for various lag times was computed from the extracted particle positions and fit to a line to extract the diffusion coefficient in MATLAB (The MathWorks; Natick, MD).

Repletion with fluorescent cholesterol analogs

RBL-2H3 cells were depleted of cholesterol using Methyl-β-cyclodextrin (MβCD; Sigma; St. Louis, MO) and then repleted with either fluorescein isothiocyanate (FITC)-cholesteryl or NBD-6 cholesterol (Avanti Lipids; Alabaster, AL) using a modified protocol optimized for RBL-2H3 cells (31). Briefly, cells were depleted with 10 mM MβCD in media supplemented with 1% fatty acid free BSA for 30 min followed with repletion using a mixture of unlabeled cholesterol, fluorescent cholesterol, and 5 mM MβCD in media supplemented with fatty acid free BSA for 30 min. FITC-cholesteryl was synthesized through monoacylation of PEG diamine with cholesteryl chloroformate followed by reaction with a fluorescein isothiocyante isomer.

Transmission electron microscopy

Gold grids were coated with formvar and carbon, glow discharged and treated to present mobile (DNP lipid bilayers) or immobilized (EGS- DNP_{24}-BSA) ligands. IgE-primed cells were settled onto grids to interact with ligand for designated periods. Samples were then fixed lightly using 0.4% paraformaldehyde and swollen in a hypotonic buffer (32). Tops of cells were gently blown from the surface with a stream of buffer, leaving behind adherent

membrane sheets. Sheets were sequentially labeled with primary antibodies and gold-conjugated secondary antibodies, stained with tannic acid and uranyl acetate, air dried, and imaged on a Hitachi 7500 TEM.

Analysis of gold particle distribution and Pearson's coefficient

Digital TEM images were analyzed with an ImageJ plugin customized to find and count coordinates of two sizes of gold particles (33). Hopkins tests were performed on coordinates to determine if particles were clustered and Ripley's K bivariate function was utilized to evaluate co-clustering (33, 34). Determinations of fluorescence overlap in dual label cholesterol experiments were performed with the ImageJ JACoP plugin (authored by Fabrice P. Cordelieres) for Pearson's coefficient (35).

Results

Surfaces presenting mobile or immobilized DNP

A variety of surfaces were designed to characterize interaction of IgE-primed RBL-2H3 cells with either mobile or immobilized DNP ligand (illustrated in Figure 1A). Homo-bifunctional crosslinkers were used to covalently attach either DNP_{24}-BSA or DNP-lysine to poly-lysine-coated glass coverslips, generating surfaces presenting immobilized polyvalent or monovalent ligands. Mobile ligand surfaces consisted of bilayers formed from vesicle fusion of DNP-lipid:POPC liposomes. Assuming the area a single phosphocholine occupies is 0.71 nm^2 (36, 37), approximately 1.4×10^6 phospholipids would occupy the upper leaflet in a bilayer uniformly covering a μm^2 area surface. By extension, the maximal number of DNP haptens presented to cells by bilayers incorporating 5–25 mol% DNP-lipid would range from $0.7–3.5 \times 10^5$ in the same area. It is possible that this is still a slight overestimate, if some amount of DNP is folded into the membrane (19). Importantly, the uniformity of the bilayers was demonstrated using Atomic Force Microscopy (AFM; Supplemental Figure 1) where a 3 nm depth for all bilayers tested was reproducibly measured. Diffusion of lipids in the surface-bound bilayers was confirmed through both single particle tracking and fluorescence recovery after photobleaching (FRAP), as described in methods. The diffusion coefficients for Alexa 488-labeled IgE (IgE^{AF488}) bound to the DNP-lipid ranged from 0.5–1 $\mu m^2/s$ for bilayers incorporating the lipid at 5 or 25 mol percent (Figure 1B). FRAP was performed on bilayers that also included the fluorescent lipid BODIPY-DHPE (3 mol%) in addition to DNP-lipid, demonstrating that recovery of the bleached spot was complete within 0.6 sec (Figure 1C). The BODIPY-DHPE exhibited a slightly faster diffusion coefficient (0.9–1.9 $\mu m^2/s$) than DNP-lipid/IgE^{AF488} complexes, potentially explained by the added size of IgE bound to the lipid. As expected, single particle tracking experiments showed that IgE^{AF488} bound to DNP^{24}-BSA remained immobile after EGS-mediated crosslinking to poly-lysine coated glass surfaces (Figure 1B).

Mast cell synapse develops upon interaction of IgE-FcεRI complex with mobile, monovalent ligand

We next evaluated the dynamics of receptor redistributions upon contact with surface-bound ligands by real-time TIRF imaging of FcεRI primed with $IgE^{Alexa488}$. Cells were added to imaging chambers containing coverslips with surface bound ligands at low enough concentration to avoid confluency. Indepedent epifluorescent microscopy experiments clarified that >80% of cells added in this manner contacted and adhered to each surface within 12 minutes. Representative images from TIRF experiments are shown in Figure 2A. Receptor membrane dynamics differed depending on the mobility of the ligand with which they were engaged. Interaction of cells with mobile ligand (DNP-lipid incorporated into a bilayer) over an extended period resulted in formation of a large, centralized region of

receptors in the ventral membrane (Figure 2A, left column). As may be seen in Supplemental Movie 1 (cluster tracking with the ImageJ Manual Tracking plugin can be seen in Supplemental Figure 2B), the IgE receptors coalesce in the central region of contact with the mobile ligand surface, similar to the behavior of TCR clusters previously reported (38, 39). The appearance and distribution of receptors in contact with DNP_{24}-BSA crosslinked to the surface (immobilized ligand) was markedly different, resulting in rapid formation of stable, moderately-sized clusters consistent with diffusional trapping by the immobilized polyvalent ligand (Figure 2A, center column; Supplemental Movie 2). Disappearance of receptor fluorescence on the DNP_{24}-BSA surfaces occurred with repetitive TIRF laser exposure. This was due to photobleaching as receptor fluorescence could still be detected in cells under the same conditions not exposed to repeated laser illumination (Figure 2A, inset of 12 min DNP-BSA-EGS column). Increased photobleaching on the DNP_{24}-BSA surfaces is most likely due to a higher production of reactive oxygen species from this surface as compared to bilayer or DNP-lysine coated surfaces.

To ensure that receptor patterning upon contact with bilayer-incorporated DNP was not due solely to ligand monovalency rather than mobility, receptor morphology was also imaged upon contacting immobilized DNP-lysine (Figure 2A, right column). The immobilized, monovalent ligand neither induced large, coalesced receptor “synapses” seen with mobile ligand nor the scattered receptor clustering patterns seen with immobilized polyvalent ligand (DNP_{24}-BSA).

Our laboratory has developed gold nanoparticle labeling and TEM imaging of native membrane sheets as a method to evaluate the topographical distributions of receptors and signaling adaptors with nanometer scale resolution (40). The series of TEM images in Figure 2B report receptor distributions on the adherent membranes after IgE-primed cells were allowed to settle on grids coated with mobile (Figure 2B, top), immobilized ligand (Figure 2B, middle), or with no ligand (Figure 2B, bottom). In this procedure, adherent cells were briefly fixed with paraformaldehyde followed by removal of the top of the cell (41, 42). Resulting membrane sheets on grids were fixed, then labeled with immunogold reagents specific for the FcεRI β subunit carboxy terminus (Figure 2B). Typically, by comparison to grids without ligand, grids presenting either mobile or immobilized ligands had increased total numbers of receptors at the adherent surface presumably due to ligand-mediated capture of receptors diffusing into the region from the remainder of the cell membrane. However, consistent with the TIRF imaging results, the nanoscale patterns of receptor distributions were quite different for each surface examined. On the mobile surface, receptors were found in dense, extensive clusters with a distinct edge (marked with a thin black line in Figure 2B, top) between the micron-size receptor cluster and neighboring, receptor-free membrane. On the immobile surface, receptor clusters were more numerous, smaller and irregularly spaced. Results of the Hopkins spatial statistic test, illustrated by graphs below each TEM image, confirmed that the distribution of receptors is significantly non-random under all conditions. The greater right-shift in the Hopkins test for the case of the DNP-lipid (mobile) reflects the larger cluster size under this condition.

Engagement with mobile ligand on lipid bilayers initiates a secretion response

Degranulation assays were performed to characterize β-hexosaminidase release from cells engaged by mobile and immobile ligand. Results, plotted in Figure 2C, are expressed as a percent of total lysosomal granule β-hexosaminidase content. Interaction of IgE-FcεRI with multivalent, immobilized ligand (DNP_{24}-BSA) resulted in degranulation at levels equivalent to that attained by stimulating cells in solution with DNP_{24}-BSA. Immobilized, monovalent DNP-lysine did not result in β-hexosaminidase release. Remarkably, degranulation was significant after settling of IgE primed mast cells onto 10 or 25 mol% DNP-lipid bilayers where ligand was mobile, monovalent and not capable of initiating receptor crosslinking.

Receptors within the synaptic region on mobile ligand remain mobile

The rapid photobleaching of receptors trapped on immobilized ligand (Figure 2A, middle column) suggested that imaging of fluorescence recovery after photobleaching (FRAP) would be a useful technique to further evaluate overall receptor movements when engaged with mobile ligand at the synaptic surface. Receptor fluorescence at the synaptic region remains dynamic (as seen in Supplementary Movie 1), making selection of a FRAP region difficult. For this reason, a larger region was selected (Figure 2D, main panel, dashed outline) because of its relative flattening and distance from the nucleus. The three images at right report the lack of fluorescence in this area immediately after bleaching, followed by recovery at 6 and 8 min post-bleach. Thus, the data demonstrate that receptors engaging mobile ligand at the adherent surface also remain mobile. In support of this conclusion, Table I reports diffusion coefficients derived from experiments tracking $IgE^{Alexa488}$-FcεRI receptor clusters (five on each surface) at early timepoints on immobilized and mobile ligand imaged with TIRF. This table also reports the expected immobility of receptors bound to DNP_{24}-BSA crosslinked to the surface.

Actin reorganization differs on mobile and immobilized ligand surfaces

Actin rings have previously been reported to form at the periphery of the T cell synapse (39, 43). We used GFP-actin transfected RBL-2H3 cells and rhodamine phalloidin immunofluorescent labeling to evaluate actin reorganization (Figure 3). TIRF imaging of GFP-actin cells indicated that actin became more concentrated at the cell periphery (ring-like) after cells settled onto surfaces containing mobile ligand (Figure 3A, middle row), despite the lack of integrin binding partners within the bilayer (39). We observed this structural change in >90% of the cells contacting the bilayer. Fixation and staining of cells stimulated with mobile ligand with rhodamine phalloidin resulted in a similar observation (Figure 3B, top row). On immobilized surfaces, an actin network surrounded receptor clusters consistent with previously described actin corrals that restrict receptor movements in unactivated cells (29) (Figure 3A, bottom row). Labeling for rhodamine phalloidin on cells fixed after stimulation with immobilized ligand showed diffuse actin staining throughout the central portion of the contacting membrane (Figure 3B, bottom row) similar to previously reported results (44). Visualization of immunofluorescent labeling was performed using confocal microscopy. TEM images of the corresponding cytoskeleton ultrastructure under each condition are shown in Figure 3C. Taken at relatively low magnification to visualize a larger portion of the membrane sheet, these images showed bundles of cytoskeletal fibers positioned at the edges of membrane adhering to mobile ligands (Figure 3C, boxed region, bottom image) and an extensive meshwork of fine, filamentous structures on membrane adhering to surfaces presenting immobilized ligand (Figure 3C, boxed region, top image).

Cholesterol associates more readily with receptors bound to mobile ligand

Previous work has strongly implicated cholesterol in the integrity and function of receptor clusters (34, 45–48). To study cholesterol dynamics during receptor reorganization upon binding to the two types of surfaces, RBL-2H3 cells were depleted of cholesterol by methyl-β cyclodextrin (MβCD) treatment and then repleted with a fluorescent cholesterol analog (FITC-cholesterol; illustrated in Figure 4A). In addition to direct imaging of the fluorescent cholesterol, we used anti-FITC antibodies combined with TEM and fluorescence-based flow cytometry techniques to 1) confirm incorporation of the cholesterol derivative into the plasma membrane and 2) determine the orientation and distribution of FITC-cholesterol in outer and inner leaflets of the lipid bilayer. Table II reports results of a flow cytometry based assay to measure the differences in mean fluorescence intensity for cells loaded for 30 min with FITC-cholesterol, followed with washing alone or washing plus quenching by the addition of anti-FITC monoclonal antibodies to the extracellular buffer. Quenching of

fluorescence of IgE^{FITC} bound to RBL-2H3 cells served as a control for this assay. The significant loss of fluorescence (>60%) indicates that a large fraction of the FITC-cholesterol resides at least initially in the outer leaflet with the FITC tag extending into the aqueous space where it is accessible to antibodies. Importantly, both live cell and TEM imaging demonstrate the differential association of labeled cholesterol with receptors engaged with either mobile or immobilized ligands. TIRF imaging of RBL-2H3 cells repleted with FITC-cholesterol demonstrated increased overlap of cholesterol rich regions with receptors when cells contacted mobile ligand (Figure 4B, middle row), as compared to surfaces presenting immobilized ligand. Pearson's coefficient (35) was performed to determine overlap of fluorescent signal from each channel (Figure 4B, bracketed numbers), confirming increased colocalization of cholesterol and receptor complexes on the mobile ligand. In contrast, there was decreased fluorescence overlap between receptors and cholesterol when cells were bound to immobilized ligand (Figure 4B, bottom row). To demonstrate that colocalization was not due to the use of FITC-cholesterol, similar results were obtained in cells repleted with an alternative fluorescent cholesterol analog, NBD-6 cholesterol (Supplementary Figure 3). TEM images of membrane sheets from cells stimulated with either immobilized or mobile ligand are consistent with TIRF imaging data (Figure 4C). Membrane sheets were double-labeled with anti-FcεRI β (12 nm) and anti-FITC (6 nm) immunogold reagents. Since antibody was applied after ripping and fixation, and access to the space between the grid and the membrane is limited, we interpret the anti-FITC label as evidence that a portion of FITC-cholesterol has flipped and become incorporated into the inner leaflet of the bilayer. Membrane sheets isolated from cells contacting mobile ligand (Figure 4C, top) demonstrate the micron-size FcεRI clusters are exceptionally rich in cholesterol; this conclusion is supported by the results of Ripley's bivariate testing (inset) demonstrating labels for the receptor and cholesterol are statistically co-clustered. By comparison, there is no significant colocalization between FITC-cholesterol and FcεRI gold labels in membrane sheets prepared from cells activated by immobilized ligand (Figure 4C, bottom). Ripley's bivariate tests (insets) confirm these conclusions. The Ripley's bivarate test for the mobile ligand example shows the red data line is well above the confidence interval as proof of strong colocalization. In contrast, for the immobilized ligand example, the red data line falls well *below* the confidence interval indicating marked segregation of the two labels within the membrane. The implications of this remarkable difference are discussed below.

LAT segregates from FcεRI clusters in membranes contacting mobile or immobilized ligand

TEM labeling of membrane sheets from RBL-2H3 cells settled onto mobile (DNP-lipid) or immobilized (DNP_{24}-BSA) ligand was performed to evaluate the relative distributions of the protein, Linker for Activation of T-cells (LAT), an important adaptor in the FcεRI signaling pathway (Figure 5). As a dually palmitoylated, transmembrane protein, LAT has the characteristics of a "raft" marker (49). Sheets were double-labeled for FcεRI β (12 nm gold) and LAT (6 nm gold) after settling onto surfaces for six minutes. Counts of LAT label on membrane sheets from mobile (Figure 5A, top panel) and immobilized (Figure 5A, bottom panel) ligand were performed (data not shown) and the general trend is higher overall number of LAT on membranes isolated from mobile substrates. Membranes from both substrates indicated exclusion of LAT domains from FcεRI clusters, confirmed by Ripley's bivariate testing (Figure 5A, inset graphs, where the red data line falls below the confidence interval). It is interesting to note that, while maintaining a clear segregation, LAT and receptor clusters on surfaces presenting mobile ligand can be close neighbors. This is indicated by the red data line in the Ripley's analysis, which reverses direction and crosses the confidence interval at a distance in the range of 100–150 nm. These results are consistent with our earlier work labeling membranes for LAT after stimulation with soluble DNP_{24}-

BSA (50). To verify that LAT is activated under these conditions, cells were fixed and labeled with anti-phosphoLAT antibodies for epifluorescence (Figure 5B). It is worth noting that only the high resolution TEM imaging can accurately capture the spatial separation between phosphoLAT and FcεRI bound to either immobilized or mobile antigen; this is explained by the resolution of the light microscope being limited to >250 nm while the TEM images revealed proximity of segregated clusters (as close as 100–150 nm).

Discussion

The current paradigm for FcεRI signal initiation requires that IgE-bound receptors be directly crosslinked into aggregates by multivalent ligand. By comparison to antigens with a valency of at least 3, soluble dimerizing ligands are often poor at activating FcεRI, although this varies with both spacing of the haptens and overall ligand concentration (51–53). However, early work by McConnell (54, 55) and McClosky (18) showed that vesicles and lipid monolayers bearing monovalent hapten-lipid conjugates could initiate a minimal signal. Here, we revisit this subject with a combination of high resolution imaging techniques and show that engagement of IgE-FcεRI with mobile, monovalent hapten at a bilayer interface results in formation of a mast cell synapse that is densely packed with thousands of mobile receptors.

It was demonstrated recently that small, crosslinked FcεRI clusters can remain mobile and signaling competent (51, 56), suggesting that immobilization and large cluster formation are not required for successful signal propagation in response to ligand binding. Remarkably, the results reported here show that monovalent ligand presented in the context of a supported lipid bilayer is also capable of inducing significant degranulation in IgE-primed mast cells, although to a lesser degree than is seen with soluble or immobilized multivalent ligand. There are at least two possible explanations for this observation. The first explanation is that binding of the surface-bound monovalent ligand alone induces a force that promotes a conformational change in the receptor, permitting recruitment of cytoplasmic signaling partners (Lyn, Syk) to the FcεRI cytoplasmic tails. More likely, signaling results because diffusion-mediated trapping at the synapse results in such high density of mobile receptors. In this scenario, there are sufficient collisions between neighboring receptors to promote transient oligomerization and transphosphorylation of FcεRI ITAMS by Lyn. We favor the latter hypothesis, since binding of receptors to immobilized monovalent haptens on surfaces should also exert significant force and yet this method failed to result in mast cell signaling to degranulation (Figure 1C). We note, however, the immobilized, monovalent haptens were likely to be randomly distributed on the substrate with large spatial separation. Thus, it remains possible that the two mechanisms work in tandem. Since conformational changes have been implicated in triggering signaling by other ITAM-bearing immunoreceptors (16, 57, 58), further work is needed to definitively resolve this issue.

It has been over a decade since the first descriptions of the immunological synapse between T cells and APCs (59–62), marked by dramatic polarization of T cells and central clusters of TCRs surrounded by a ring of adhesion molecules. Engagement of BCR with antigens on the surface of another cell can also lead to B cell polarization, along with many of the hallmarks of the T cell synapse (63). The immunological synapse field continues to advance, including new concepts regarding the signal amplification properties provided by the synapse platform and the sustainability of signaling through newly arriving receptors (15, 64). Here, we show that mast cells are also capable of forming a synapse on lipid bilayers and postulate that this is a fundamental capability of most leukocytes. We report the first electron microscopy images of immunoreceptors in contact with ligand-presenting bilayers, providing high resolution snapshots of synapse organization. It is notable that mast cells can

mobilize a synapse on high densities of mobile lipid alone. In physiological settings, we speculate that activation of integrins accompanies FcεRI stimulus (65), facilitating firm adhesion as it does in T cells (66).

Multiple cellular components have been implicated in synapse organization, including lipid composition (1, 45, 67), the cytoskeleton (43), and cytoplasmic scaffolding proteins (68). The role of cholesterol-rich lipid rafts in cell signaling remains an active field of study (69–72). Early work by Baird, Holowka and colleagues described movement of FcεRI into detergent-resistant membrane domains after crosslinking with soluble polyvalent ligand (34, 45–48). Our recent lipidomics study concluded that the lipid environment near large FcεRI aggregates, also crosslinked by soluble ligand, is nearly 50% cholesterol (48). In the present work, we used fluorescent cholesterol analogs (31, 73) to image the relationship of cholesterol-rich domains to IgE receptors in the context of the mast cell synapse. Activation of IgE-primed mast cells with mobile, monovalent ligand results in coalescence of cholesterol and receptors within the synaptic region, a result not seen with immobilized ligand. These data are difficult to interpret in the context of current models of the membrane. For example, if cholesterol is so closely associated with the FcεRI as to form part of its lipid shell, a hypothesis originally proposed by Anderson and Jacobson (74), one would expect it to strongly partition with receptors regardless of how FcεRI activation occurs. Yet, cholesterol only partitions with receptor on the surface presenting the mobile ligand. It seems reasonable to speculate that receptors and cholesterol are instead weakly associated, and the diffusive properties of cholesterol favor their dissociation if the receptor becomes immobilized. This postulate is consistent with the work of Sheets and colleagues, who noted only transient association of FcεRI aggregates with a fluorescent lipid raft probe (75).

LAT, a dually palmitoylated protein that serves as a scaffold in the FcεRI signaling cascade, is often considered a raft marker (49). We previously showed that LAT clusters enlarge in size after FcεRI activation with soluble polyvalent ligand but segregate strongly from FcεRI clusters (34, 76, 77). Given the remarkable association between cholesterol and FcεRI engaged with mobile ligand at synapse, we also evaluated the potential for greater colocalization between FcεRI and LAT under these conditions. Data presented in Figure 6, which show that LAT clusters still segregate from the densely packed FcεRI, cholesterol-rich domains at the mobile synapse, suggest that LAT clusters are not equivalent to cholesterol rafts.

Actin reorganization also contributes to formation of the immunological synapse and TCR localization (43). Similar cytoskeletal structural changes occur when mast cells contact mobile ligand to form a synapse (Figure 3). When mast cells are primed with a heterogenous IgE population (anti-dansyl and anti-DNP) and settled onto mobile ligand (DNP-lipid), IgE-FcεRI complexes that do not recognize the bilayer-incorporated hapten are selectively excluded from the synaptic region (data not shown). This indicates an active selection process for receptor incorporation into the synapse rather than a generalized membrane flow. It is possible that the cytoskeleton and its associated proteins may be involved in this process, a hypothesis that will require further investigation.

This report presents the first detailed characterization of the mast cell synapse. Spatial organization and signaling competency are clearly distinct when receptors are engaged with mobile or immobile ligands on surfaces. This work sets the stage to explore roles for membrane reorganization when mast cells engage in direct contact with other immune cells. Given recent evidence for mast cells as *bona fide* immune modulatory cells (21–23), synapses between mast cells and other leukocytes are likely have functional consequences during immune responses.

Supplementary Material

Refer to Web version on PubMed Central for supplementary material.

Acknowledgments

Confocal images in this paper were generated in the University of New Mexico Cancer Center Fluorescence Microscopy Facility. We acknowledge Ryan Davis for his assistance with hyperspectral confocal imaging, Shannon Coffeil and Nalini Shenoy for preparation of fluorescent cholesterol analogs, and Alan Burns for his contributions to the initial funding of this project. We thank Dr. Gabriel Montano at the Center for Integrated NanoTechnologies, Los Alamos National Laboratories for performing the Atomic Force Microscopy in the supplemental section.

Abbreviations used in this paper

FcεRI	high affinity IgE receptor
LAT	linker for activation of T cells
RBL-2H3	rat basophilic leukemia 2H3 cell line
Syk	spleen tyrosine kinase
TEM	transmission electron microscopy
TIRF	total internal reflection fluorescence
IgE	Immunoglobulin E
SH2	Src homology domains 2
MIRR	multi-subunit immunorecognition receptor

References

1. Oliver JM, Pfeiffer JR, Surviladze Z, Steinberg SL, Leiderman K, Sanders ML, Wofsy C, Zhang J, Fan H, Andrews N, Bunge S, Boyle TJ, Kotula P, Wilson BS. Membrane receptor mapping: the membrane topography of Fc(epsilon)RI signaling. Subcell Biochem. 2004; 37:3–34. [PubMed: 15376617]
2. Sada K, Zhang J, Siraganian RP. SH2 domain-mediated targeting, but not localization, of Syk in the plasma membrane is critical for FcepsilonRI signaling. Blood. 2001; 97:1352–1359. [PubMed: 11222380]
3. Zhang J, Billingsley ML, Kincaid RL, Siraganian RP. Phosphorylation of Syk activation loop tyrosines is essential for Syk function. An in vivo study using a specific anti-Syk activation loop phosphotyrosine antibody. J Biol Chem. 2000; 275:35442–35447. [PubMed: 10931839]
4. Gilfillan AM, Rivera J. The tyrosine kinase network regulating mast cell activation. Immunol Rev. 2009; 228:149–169. [PubMed: 19290926]
5. Oliver JM, Burg DL, Wilson BS, McLaughlin JL, Geahlen RL. Inhibition of mast cell Fc epsilon R1-mediated signaling and effector function by the Syk-selective inhibitor, piceatannol. J Biol Chem. 1994; 269:29697–29703. [PubMed: 7961959]
6. Turner M, Schweighoffer E, Colucci F, Di Santo JP, Tybulewicz VL. Tyrosine kinase SYK: essential functions for immunoreceptor signalling. Immunol Today. 2000; 21:148–154. [PubMed: 10689303]
7. Zhang J, Berenstein EH, Evans RL, Siraganian RP. Transfection of Syk protein tyrosine kinase reconstitutes high affinity IgE receptor-mediated degranulation in a Syk-negative variant of rat basophilic leukemia RBL-2H3 cells. J Exp Med. 1996; 184:71–79. [PubMed: 8691151]
8. Hernandez-Hansen V, Smith AJ, Surviladze Z, Chigaev A, Mazel T, Kalesnikoff J, Lowell CA, Krystal G, Sklar LA, Wilson BS, Oliver JM. Dysregulated FcepsilonRI signaling and altered Fyn and SHIP activities in Lyn-deficient mast cells. J Immunol. 2004; 173:100–112. [PubMed: 15210764]

9. Depoil D, Weber M, Treanor B, Fleire SJ, Carrasco YR, Harwood NE, Batista FD. Early events of B cell activation by antigen. Sci Signal. 2009; 2(pt 1)
10. Geahlen RL. Syk and pTyr'd: Signaling through the B cell antigen receptor. Biochim Biophys Acta. 2009; 1793:1115–1127. [PubMed: 19306898]
11. Smith-Garvin JE, Koretzky GA, Jordan MS. T cell activation. Annu Rev Immunol. 2009; 27:591–619. [PubMed: 19132916]
12. Cairo CW, Mirchev R, Golan DE. Cytoskeletal regulation couples LFA-1 conformational changes to receptor lateral mobility and clustering. Immunity. 2006; 25:297–308. [PubMed: 16901728]
13. Dustin ML. A dynamic view of the immunological synapse. Semin Immunol. 2005; 17:400–410. [PubMed: 16266811]
14. Groves JT, Dustin ML. Supported planar bilayers in studies on immune cell adhesion and communication. J Immunol Methods. 2003; 278:19–32. [PubMed: 12957393]
15. Huppa JB, Davis MM. T-cell-antigen recognition and the immunological synapse. Nat Rev Immunol. 2003; 3:973–983. [PubMed: 14647479]
16. Tolar P, Hanna J, Krueger PD, Pierce SK. The constant region of the membrane immunoglobulin mediates B cell-receptor clustering and signaling in response to membrane antigens. Immunity. 2009; 30:44–55. [PubMed: 19135393]
17. Tolar P, Sohn HW, Pierce SK. Viewing the antigen-induced initiation of B-cell activation in living cells. Immunol Rev. 2008; 221:64–76. [PubMed: 18275475]
18. McCloskey MA, Poo MM. Contact-induced redistribution of specific membrane components: local accumulation and development of adhesion. J Cell Biol. 1986; 102:2185–2196. [PubMed: 2423534]
19. McConnell HM, Watts TH, Weis RM, Brian AA. Supported planar membranes in studies of cell-cell recognition in the immune system. Biochim Biophys Acta. 1986; 864:95–106. [PubMed: 2941079]
20. Silverman MA, Shoag J, Wu J, Koretzky GA. Disruption of SLP-76 interaction with Gads inhibits dynamic clustering of SLP-76 and FcepsilonRI signaling in mast cells. Mol Cell Biol. 2006; 26:1826–1838. [PubMed: 16479002]
21. Perrigoue JG, Saenz SA, Siracusa MC, Allenspach EJ, Taylor BC, Giacomin PR, Nair MG, Du Y, Zaph C, van Rooijen N, Comeau MR, Pearce EJ, Laufer TM, Artis D. MHC class II-dependent basophil-CD4+ T cell interactions promote T(H)2 cytokine dependent immunity. Nat Immunol. 2009; 10:697–705. [PubMed: 19465906]
22. Sokol CL, Chu NQ, Yu S, Nish SA, Laufer TM, Medzhitov R. Basophils function as antigen-presenting cells for an allergen-induced T helper type 2 response. Nat Immunol. 2009; 10:713–720. [PubMed: 19465907]
23. Yoshimoto T, Yasuda K, Tanaka H, Nakahira M, Imai Y, Fujimori Y, Nakanishi K. Basophils contribute to T(H)2-IgE responses in vivo via IL-4 production and presentation of peptide-MHC class II complexes to CD4+ T cells. Nat Immunol. 2009; 10:706–712. [PubMed: 19465908]
24. Liu FT, Bohn JW, Ferry EL, Yamamoto H, Molinaro CA, Sherman LA, Klinman NR, Katz DH. Monoclonal dinitrophenyl-specific murine IgE antibody: preparation, isolation, and characterization. J Immunol. 1980; 124:2728–2737. [PubMed: 7373045]
25. Seagrave J, Pfeiffer JR, Wofsy C, Oliver JM. Relationship of IgE receptor topography to secretion in RBL-2H3 mast cells. J Cell Physiol. 1991; 148:139–151. [PubMed: 1830592]
26. Smith AJ, Pfeiffer JR, Zhang J, Martinez AM, Griffiths GM, Wilson BS. Microtubule-dependent transport of secretory vesicles in RBL-2H3 cells. Traffic. 2003; 4:302–312. [PubMed: 12713658]
27. Yguerabide J, Schmidt JA, Yguerabide EE. Lateral mobility in membranes as detected by fluorescence recovery after photobleaching. Biophys J. 1982; 40:69–75. [PubMed: 7139035]
28. Sinclair MB, Haaland DM, Timlin JA, Jones HD. Hyperspectral confocal microscope. Appl Opt. 2006; 45:6283–6291. [PubMed: 16892134]
29. Andrews NL, Lidke KA, Pfeiffer JR, Burns AR, Wilson BS, Oliver JM, Lidke DS. Actin restricts FcepsilonRI diffusion and facilitates antigen-induced receptor immobilization. Nat Cell Biol. 2008; 10:955–963. [PubMed: 18641640]

30. Sage D, Neumann FR, Hediger F, Gasser SM, Unser M. Automatic tracking of individual fluorescence particles: application to the study of chromosome dynamics. IEEE TransImage Process. 2005; 14:1372–1383.

31. Sato SB, Ishii K, Makino A, Iwabuchi K, Yamaji-Hasegawa A, Senoh Y, Nagaoka I, Sakuraba H, Kobayashi T. Distribution and transport of cholesterol-rich membrane domains monitored by a membrane-impermeant fluorescent polyethylene glycol-derivatized cholesterol. J Biol Chem. 2004; 279:23790–23796. [PubMed: 15026415]

32. Sanan DA, Anderson RG. Simultaneous visualization of LDL receptor distribution and clathrin lattices on membranes torn from the upper surface of cultured cells. J Histochem Cytochem. 1991; 39:1017–1024. [PubMed: 1906908]

33. Zhang J, Leiderman K, Pfeiffer JR, Wilson BS, Oliver JM, Steinberg SL. Characterizing the topography of membrane receptors and signaling molecules from spatial patterns obtained using nanometer-scale electron-dense probes and electron microscopy. Micron. 2006; 37:14–34. [PubMed: 16081296]

34. Wilson BS, Steinberg SL, Liederman K, Pfeiffer JR, Surviladze Z, Zhang J, Samelson LE, Yang LH, Kotula PG, Oliver JM. Markers for detergent-resistant lipid rafts occupy distinct and dynamic domains in native membranes. Mol Biol Cell. 2004; 15:2580–2592. [PubMed: 15034144]

35. Manders EM, Stap J, Brakenhoff GJ, van Driel R, Aten JA. Dynamics of three dimensional replication patterns during the S-phase, analysed by double labelling of DNA and confocal microscopy. J Cell Sci. 1992; 103(Pt 3):857–862. [PubMed: 1478975]

36. Petrache HI, Dodd SW, Brown MF. Area per lipid and acyl length distributions in fluid phosphatidylcholines determined by (2)H NMR spectroscopy. Biophys J. 2000; 79:3172–3192. [PubMed: 11106622]

37. Higgins MJ, Polcik M, Fukuma T, Sader JE, Nakayama Y, Jarvis SP. Structured water layers adjacent to biological membranes. Biophys J. 2006; 91:2532–2542. [PubMed: 16798815]

38. Campi G, Varma R, Dustin ML. Actin and agonist MHC-peptide complex dependent T cell receptor microclusters as scaffolds for signaling. J Exp Med. 2005; 202:1031–1036. [PubMed: 16216891]

39. Kaizuka Y, Douglass AD, Varma R, Dustin ML, Vale RD. Mechanisms for segregating T cell receptor and adhesion molecules during immunological synapse formation in Jurkat T cells. Proc Natl Acad Sci U S A. 2007; 104:20296–20301. [PubMed: 18077330]

40. Wilson, BS.; Pfeiffer, JR.; Raymond-Stintz, MA.; Lidke, D.; Andrews, N.; Zhang, J.; Yin, W.; Steinberg, S.; Oliver, JM. Exploring Membrane Domains Using Native Membrane Sheets and Transmission Electron Microscopy. In: McIntosh, T., editor. Methods in Molecular Biology: Lipid Rafts. Humana Press; 2008. p. 245-261.

41. Avnur Z, Geiger B. Substrate-attached membranes of cultured cells isolation and characterization of ventral cell membranes and the associated cytoskeleton. J Mol Biol. 1981; 153:361–379. [PubMed: 7040683]

42. Pfeiffer JR, Oliver JM. Tyrosine kinase-dependent assembly of actin plaques linking Fc epsilon R1 cross-linking to increased cell substrate adhesion in RBL-2H3 tumor mast cells. J Immunol. 1994; 152:270–279. [PubMed: 7504712]

43. Dustin ML, Cooper JA. The immunological synapse and the actin cytoskeleton: molecular hardware for T cell signaling. Nat Immunol. 2000; 1:23–29. [PubMed: 10881170]

44. Psatha M, Koffer A, Erent M, Moss SE, Bolsover S. Calmodulin spatial dynamics in RBL-2H3 mast cells. Cell Calcium. 2004; 36:51–59. [PubMed: 15126056]

45. Davey AM, Walvick RP, Liu Y, Heikal AA, Sheets ED. Membrane order and molecular dynamics associated with IgE receptor cross-linking in mast cells. Biophys J. 2007; 92:343–355. [PubMed: 17040981]

46. Pyenta PS, Holowka D, Baird B. Cross-correlation analysis of inner-leaflet anchored green fluorescent protein co-redistributed with IgE receptors and outer leaflet lipid raft components. Biophys J. 2001; 80:2120–2132. [PubMed: 11325715]

47. Stauffer TP, Meyer T. Compartmentalized IgE receptor-mediated signal transduction in living cells. J Cell Biol. 1997; 139:1447–1454. [PubMed: 9396750]

48. Surviladze Z, Harrison KA, Murphy RC, Wilson BS. FcepsilonRI and Thy-1 domains have unique protein and lipid compositions. J Lipid Res. 2007; 48:1325–1335. [PubMed: 17387221]
49. Zhang W, Trible RP, Samelson LE. LAT palmitoylation: its essential role in membrane microdomain targeting and tyrosine phosphorylation during T cell activation. Immunity. 1998; 9:239–246. [PubMed: 9729044]
50. Wilson BS, Pfeiffer JR, Surviladze Z, Gaudet EA, Oliver JM. High resolution mapping of mast cell membranes reveals primary and secondary domains of Fc(epsilon)RI and LAT. J Cell Biol. 2001; 154:645–658. [PubMed: 11489921]
51. Andrews NL, Pfeiffer JR, Martinez AM, Haaland DM, Davis RW, Kawakami T, Oliver JM, Wilson BS, Lidke DS. Small, mobile FcεRI aggregates are signaling competent. Immunity. 2009 In Press.
52. Posner RG, Geng D, Haymore S, Bogert J, Pecht I, Licht A, Savage PB. Trivalent antigens for degranulation of mast cells. Org Lett. 2007; 9:3551–3554. [PubMed: 17691795]
53. Sil D, Lee JB, Luo D, Holowka D, Baird B. Trivalent ligands with rigid DNA spacers reveal structural requirements for IgE receptor signaling in RBL mast cells. ACS Chem Biol. 2007; 2:674–684. [PubMed: 18041817]
54. Cooper AD, Balakrishnan K, McConnell HM. Mobile haptens in liposomes stimulate serotonin release by rat basophil leukemia cells in the presence of specific immunoglobulin E. J Biol Chem. 1981; 256:9379–9381. [PubMed: 7287691]
55. Weis RM, Balakrishnan K, Smith BA, McConnell HM. Stimulation of fluorescence in a small contact region between rat basophil leukemia cells and planar lipid membrane targets by coherent evanescent radiation. J Biol Chem. 1982; 257:6440–6445. [PubMed: 6804467]
56. Grodzki AC, Moon KD, Berenstein EH, Siraganian RP. FcepsilonRI-induced activation by low antigen concentrations results in nuclear signals in the absence of degranulation. Mol Immunol. 2009; 46:2539–2547. [PubMed: 19540596]
57. Gil D, Schamel WW, Montoya M, Sanchez-Madrid F, Alarcon B. Recruitment of Nck by CD3 epsilon reveals a ligand-induced conformational change essential for T cell receptor signaling and synapse formation. Cell. 2002; 109:901–912. [PubMed: 12110186]
58. Ma Z, Janmey PA, Finkel TH. The receptor deformation model of TCR triggering. FASEB J. 2008; 22:1002–1008. [PubMed: 17984179]
59. Grakoui A, Bromley SK, Sumen C, Davis MM, Shaw AS, Allen PM, Dustin ML. The immunological synapse: a molecular machine controlling T cell activation. Science. 1999; 285:221–227. [PubMed: 10398592]
60. Monks CR, Freiberg BA, Kupfer H, Sciaky N, Kupfer A. Three-dimensional segregation of supramolecular activation clusters in T cells. Nature. 1998; 395:82–86. [PubMed: 9738502]
61. Shaw AS, Dustin ML. Making the T cell receptor go the distance: a topological view of T cell activation. Immunity. 1997; 6:361–369. [PubMed: 9133415]
62. Wulfing C, Davis MM. A receptor/cytoskeletal movement triggered by costimulation during T cell activation. Science. 1998; 282:2266–2269. [PubMed: 9856952]
63. Batista FD, Iber D, Neuberger MS. B cells acquire antigen from target cells after synapse formation. Nature. 2001; 411:489–494. [PubMed: 11373683]
64. Dustin ML. T-cell activation through immunological synapses and kinapses. Immunol Rev. 2008; 221:77–89. [PubMed: 18275476]
65. Kepley CL, Youssef L, Andrews RP, Wilson BS, Oliver JM. Multiple defects in Fc epsilon RI signaling in Syk-deficient nonreleaser basophils and IL-3-induced recovery of Syk expression and secretion. J Immunol. 2000; 165:5913–5920. [PubMed: 11067953]
66. Sims TN, Dustin ML. The immunological synapse: integrins take the stage. Immunol Rev. 2002; 186:100–117. [PubMed: 12234366]
67. Holowka D, Gosse JA, Hammond AT, Han X, Sengupta P, Smith NL, Wagenknecht-Wiesner A, Wu M, Young RM, Baird B. Lipid segregation and IgE receptor signaling:a decade of progress. Biochim Biophys Acta. 2005; 1746:252–259. [PubMed: 16054713]
68. Shaw AS, Filbert EL. Scaffold proteins and immune-cell signalling. Nat Rev Immunol. 2009; 9:47–56. [PubMed: 19104498]

69. Jacobson K, Mouritsen OG, Anderson RG. Lipid rafts: at a crossroad between cell biology and physics. Nat Cell Biol. 2007; 9:7–14. [PubMed: 17199125]

70. Mondal M, Mesmin B, Mukherjee S, Maxfield FR. Sterols are mainly in the cytoplasmic leaflet of the plasma membrane and the endocytic recycling compartment in CHO cells. Mol Biol Cell. 2009; 20:581–588. [PubMed: 19019985]

71. Shaikh SR, Edidin MA. Membranes are not just rafts. Chem Phys Lipids. 2006; 144:1–3. [PubMed: 16945359]

72. Hancock JF. Lipid rafts: contentious only from simplistic standpoints. Nat Rev Mol Cell Biol. 2006; 7:456–462. [PubMed: 16625153]

73. Shaw JE, Epand RF, Epand RM, Li Z, Bittman R, Yip CM. Correlated fluorescence-atomic force microscopy of membrane domains: structure of fluorescence probes determines lipid localization. Biophys J. 2006; 90:2170–2178. [PubMed: 16361347]

74. Anderson RG, Jacobson K. A role for lipid shells in targeting proteins to caveolae, rafts, and other lipid domains. Science. 2002; 296:1821–1825. [PubMed: 12052946]

75. Davey AM, Krise KM, Sheets ED, Heikal AA. Molecular perspective of antigen-mediated mast cell signaling. J Biol Chem. 2008; 283:7117–7127. [PubMed: 18093971]

76. Lebduska P, Korb J, Tumova M, Heneberg P, Draber P. Topography of signaling molecules as detected by electron microscopy on plasma membrane sheets isolated from nonadherent mast cells. J Immunol Methods. 2007; 328:139–151. [PubMed: 17900607]

77. Wilson BS, Pfeiffer JR, Oliver JM. FcepsilonRI signaling observed from the inside of the mast cell membrane. Mol Immunol. 2002; 38:1259–1268. [PubMed: 12217393]

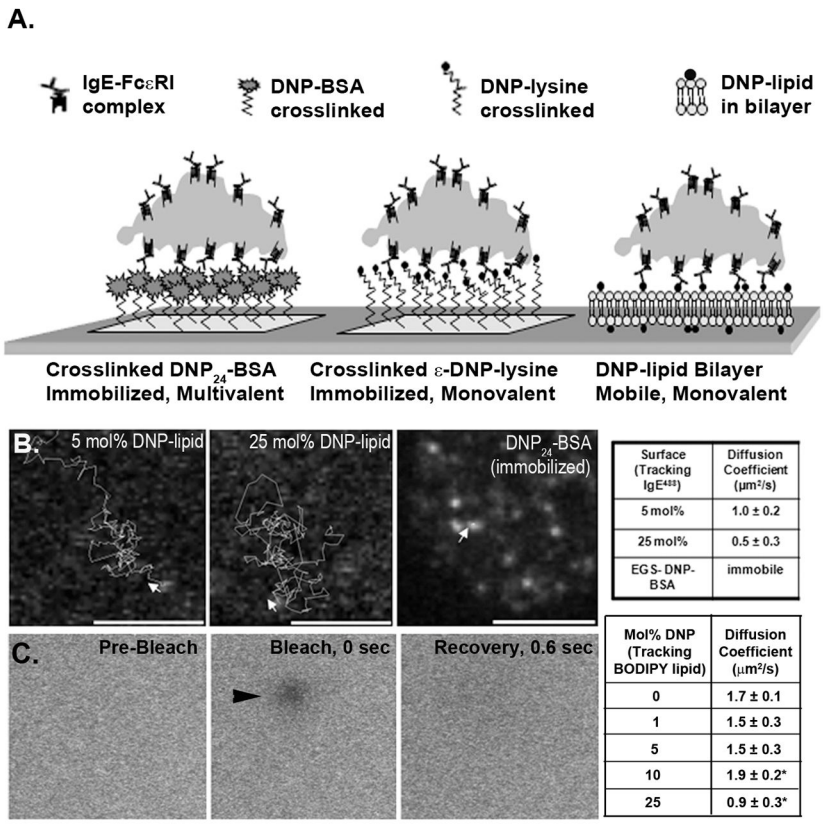

Surface (Tracking IgE^{488})	Diffusion Coefficient ($\mu m^2/s$)
5 mol%	1.0 ± 0.2
25 mol%	0.5 ± 0.3
EGS-DNP-BSA	immobile

Mol% DNP (Tracking BODIPY lipid)	Diffusion Coefficient ($\mu m^2/s$)
0	1.7 ± 0.1
1	1.5 ± 0.3
5	1.5 ± 0.3
10	1.9 ± 0.2*
25	0.9 ± 0.3*

FIGURE 1.

Illustration and characterization of surfaces. *A.* Representation of IgE-primed cells contacting different types of antigen presenting surfaces. *B.* Tracking of fluorescent IgE bound to 5 mol%, 25 mol% DNP-lipid/POPC lipid bilayers and crosslinked DNP-BSA surfaces. Arrows indicate starting point and initial direction of each track. Diffusion coefficients were calculated from tracking of IgE^{AF488} bound to each tested surface (Table at right). *C.* Sequential images of FRAP performed on a 25 mol% bilayer showing pre-bleach, bleach spot, and recovery. Calculated diffusion coefficients for each surface are indicated in the associated table. *Statistically significant with P-value ≤ 0.01; n=5.

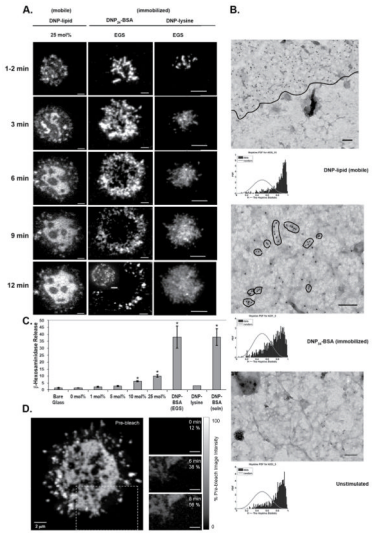

FIGURE 2.

Receptor behavior and distribution is dependent upon the type of contact surface. *A.* TIRF imaging of IgE^{AF488}-primed cells engaged with mobile (left column) or immobile (middle and right columns) ligand presenting surfaces over a 12 minute period. Images are contrast enhanced. All scale bars represent 5 μm. Disappearance of signal in the central region of the cell settled onto the EGS-DNP-BSA surface is due to photobleaching indicated by another cell imaged under similar conditions without extensive laser exposure (inset image). *B.* TEM images of membrane sheets from cells settled onto mobile (DNP-lipid in bilayer), immobilized (EGS-DNP-BSA) ligand, or non-activating surface. FcεRI β is labeled with 12 nm or 6 nm gold. Line in top panel delineates area of receptor coalescence within the membrane. Hopkins tests are located below each image for which they were performed. Images are contrast enhanced. Scale bars are 100 nm. *C.* Percent β-hexosaminadase release from cells settled onto glass, mobile ligand, immobilized ligand, or stimulated by soluble antigen. Asterisks indicate results that are significantly higher than spontaneous release (bare glass). *D.* Fluorescence recovery of a bleached portion of a synaptic region formed on a 25 mol% DNP-lipid bilayer. The region outlined in a dashed box indicates region bleached. Bleach and post-bleach images taken at 6 and 8 minute time points are in the right column. Grayscale range indicator shows amount of fluorescent recovery in each post-bleach image. All images were corrected for within-scan photobleaching by scaling to a non-bleached region of the synapse.

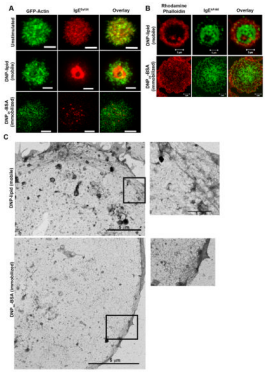

FIGURE 3.

Actin reorganization at the adherent surface is dependent upon ligand mobility. *A.* TIRF imaging of GFP-actin RBL-2H3 cells primed with IgE^{Dy520} settled onto glass, mobile (DNP-lipid) ligand, or immobilized (EGS-DNP_{24}-BSA) ligand. Scale bars are 5 μm. *B.* Confocal imaging of IgE^{AF488}-primed RBL-2H3 cells fixed with paraformaldehyde and labeled with rhodamine phalloidin. Top row is a cell settled onto a 25 mol% DNP-lipid bilayer and bottom row is a cell settled onto a DNP_{24}-BSA surface. Scale bars are 5 μm. *C.* Low magnification TEM of membrane sheets from cells bound to an EGS-DNP_{24}-BSA EM grid (top) or a bilayer coated EM grid (bottom). Boxed regions are magnified views of cytoskeletal structures for each sheet. Scale bars are 100 nm. All images are contrast enhanced.

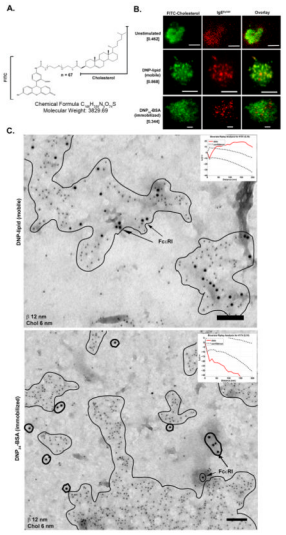

FIGURE 4.

Fluorescent cholesterol derivatives reveal strong association with mobile but not immobile FcεRI. *A.* Fluorescent cholesterol analog used in membrane repletion with a short chain PEG linker between the FITC molecule and cholesterol. *B.* TIRF imaging of RBL-2H3 cells repleted with FITC cholesterol and primed with IgE^{Dy520} after contact with glass (top row), mobile ligand (middle row), or immobilized ligand (bottom row). Pearson's coefficient calculation from each series of fluorescent images is in brackets. Scale bars are 5 μm. *C.* TEM membrane sheets from cells settled onto EM grids coated with mobile or immobilized ligand. Regions of receptor (12 nm gold) and cholesterol (6 nm gold) colocalization on the mobile surface are outlined. On the immobile surface, regions of cholesterol are outlined in a thin line while receptors are circled with a thick line. Ripley's tests for coincidence of label for FcεRI β and FITC (cholesterol) are shown as insets. Scale bars are 100 nm. All images are contrast enhanced.

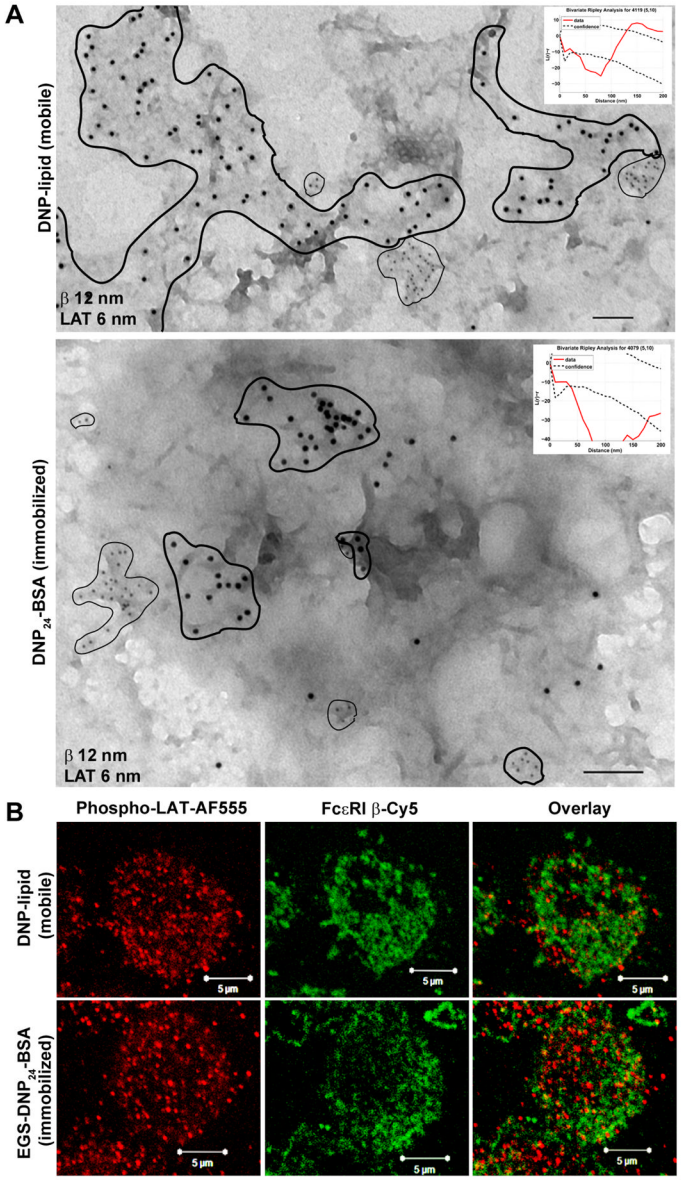

FIGURE 5.

LAT clusters do not colocalize with FcεRI at the synapse. *A.* Membrane sheets from IgE primed cells settled onto mobile (top) or immobilized (bottom) ligand for six minutes and labeled for FcεRI β (12 nm gold) or LAT (6 nm gold). LAT clusters are circled with thin lines on each sheet to indicate general cluster size and location relative to receptors (circled with thick lines). Scale bars are 100 nm. Ripley's tests for coincidence of LAT and FcεRI β label are inset in each figure. *B.* Paraformaldehyde fixed IgE^{DNP}-primed RBL-2H3 cells settled onto 25 mol% DNP-lipid (top row) or DNP_{24}-BSA (bottom row) surfaces for 6 minutes. After permeabilization, cells were dually labeled for phosphorylated LAT (AF555) and FcεRI β (Cy5; psuedocolored). Images are contrast enhanced.

Table I

Diffusion coefficients of receptor clusters when bound to mobile or immobilized DNP

Surface	Diffusion Coefficient (μm^2/sec)
DNP_{24}-BSA (immobilized)	Immobile†
25 mol% DNP-lipid (mobile)	$4.1\times10^{-3} \pm 1.6\times10^{-3}$*
10 mol% DNP-lipid (mobile)	$4.9\times10^{-3} \pm 2.1\times10^{-3}$*
5 mol% DNP-lipid (mobile)	$9.1\times10^{-3} \pm 6.9\times10^{-3}$*

*P-value ≤ 0.01; Significant compared to coefficients obtained with DNP_{24}-BSA

†Immobile as defined by a diffusion coefficient < 1.0×10^{-5} μm^2/sec

Table II

Quenching of FITC-cholesterol with monoclonal antibody

Fluorescent Label	Pre-Quench	Post-Quench
$IgE^{FITC\ (2hr\ labeling)}$	52.54	9.23
FITC-Cholesterol	97.95	36.35